Crystal Structure of NADP(H)-Dependent 1,5-Anhydro-D-fructose Reductase from *Sinorhizobium morelense* at 2.2 Å Resolution: Construction of a NADH-Accepting Mutant and Its Application in Rare Sugar Synthesis[†,‡]

Tresfore R. Dambe,[§,||] Annette M. Kühn,[⊥,#] Tatjana Brossette,[⊥] Friedrich Giffhorn,*[,⊥] and Axel J. Scheidig*[,§]

Abteilung Strukturbiologie, Fachbereich Biophysik, Universitätsklinikum des Saarlandes, D-66424 Homburg/Saar, Germany, and Lehrstuhl für Angewandte Mikrobiologie, Universität des Saarlandes, P.O. Box 151150, D-66041 Saarbrücken, Germany

Received December 20, 2005; Revised Manuscript Received June 19, 2006

ABSTRACT: Recombinant 1,5-anhydro-D-fructose reductase (AFR) from *Sinorhizobium morelense* S-30.7.5 was crystallized in complex with the cofactor NADP(H) and its structure determined to 2.2 Å resolution using selenomethionine SAD (refined R_{work} and R_{free} factors of 18.9 and 25.0%, respectively). As predicted from the sequence and shown by the structure, AFR can be assigned to the GFO/IDH/MocA protein family. AFR consists of two domains. The N-terminal domain displays a Rossmann fold and contains the cofactor binding site. The intact crystals contain the oxidized cofactor $NADP^+$, whose attachment to the cofactor binding site is similar to that of $NADP^+$ in glucose-fructose oxidoreductase (GFOR) from *Zymomonas mobilis*. Due to variations in length and sequence within loop regions L3 and L5, respectively, the adenine moiety of $NADP^+$ adopts a different orientation in AFR caused by residue Arg38 forming hydrogen bonds with the 2′-phosphate moiety of $NADP^+$ and cation−π stacking interactions with the adenine ring. Amino acid replacements in AFR (S10G, A13G, and S33D) showed that Ala13 is crucial for the discrimination between NADPH and NADH and yielded the A13G variant with dual cosubstrate specificity. The C-terminal domain contains the putative substrate binding site that was occupied by an acetate ion. As determined by analogy to GFOR and by site-directed mutagenesis of K94G, D176A, and H180A, residues Lys94, Asp176, and His180 are most likely involved in substrate binding and catalysis, as substitution of any of these residues resulted in a significant decrease in k_{cat} for 1,5-AF. In this context, His180 might serve as a general acid−base catalyst by polarizing the carbonyl function of 1,5-AF to enable the transfer of the hydride from NADPH to the substrate. Here we present the first structure of an AFR enzyme catalyzing the stereoselective reduction of 1,5-AF to 1,5-anhydro-D-mannitol, the final step of a modified anhydrofructose pathway in *S. morelense* S-30.7.5. We also emphasize the importance of the A13G variant in biocatalysis for the synthesis of 1,5-AM and related derivatives.

The sugar 1,5-anhydro-D-fructose (1,5-AF)[1] is the central intermediate of the so-called anhydrofructose pathway, an alternative starch- and glycogen-degrading pathway in bacteria, fungi, plants, and mammals. 1,5-AF originates from starch or glycogen and is produced by α-(1,4)-glucan lyase (EC 4.2.2.13), which catalyzes the release of 1,5-AF from the nonreducing end of α-(1,4)-glucans (for a review, see ref *1*). In *Escherichia coli*, higher plants, and mammalian tissues, the half-life of 1,5-AF is short as it is instantly reduced to 1,5-anhydro-D-glucitol (1,5-AG) by a specific NADPH-dependent anhydrofructose reductase (EC 1.1.1.263) (*2*). Since only a small fraction of α-(1,4)-glucans is degraded via the anhydrofructose pathway, it was assumed that 1,5-AF or 1,5-AG could play regulatory roles in glycogen metabolism (*3*−*5*). In *E. coli*, 1,5-AG promotes glycogenolysis (*6*), and in mammals, 1,5-AF or 1,5-AG stimulates insulin secretion (*7*, *8*). Although little is known about the physiological importance of 1,5-AF and 1,5-AG in human glucose homeostasis, differences in 1,5-AG serum concentrations between healthy and diabetic individuals are observed, having rendered 1,5-AG an established marker in diabetic control (*9*). Furthermore, trials have been initiated to use 1,5-AF and its derivatives against sugar metabolism disorder-related disease (*7*, *10*). To afford wider and more systematic studies on the physiological role of 1,5-AF and its derivatives in

[†] Research was supported by the European Union within the 5th framework program *NEPSA* with Contract QLK3-CT-2001-02400 (to F.G.).

[‡] Atomic coordinates and structure factor amplitudes have been deposited with the Protein Data Bank as entry 2GLX.

* To whom correspondence should be addressed. F.G.: telephone, +49-681-302-2704; fax, +49-681-302-4360; e-mail, giffhorn@mx.uni-saarland.de. A.J.S.: telephone, +49-6841-1626235; fax, +49-6841-1626251; e-mail, axel.scheidig@uniklinik-saarland.de.

[§] Abteilung Strukturbiologie, Fachbereich Biophysik, Universitätsklinikum des Saarlandes.

[||] Current address: PSF biotech AG, D-14059 Berlin, Germany.

[⊥] Lehrstuhl für Angewandte Mikrobiologie, Universität des Saarlandes.

[#] Current address: Laboratory of Immunogenetics and Allergology, CRP-Santé, 86 Val Fleuri, L-1526 Luxembourg, Luxembourg.

[1] Abbreviations: 1,5-AF, 1,5-anhydro-D-fructose; 1,5-AG, 1,5-anhydro-D-glucitol; 1,5-AM, 1,5-anhydro-D-mannitol; AFR, 1,5-anhydro-D-fructose reductase; Bistris, 2,2-bis(hydroxymethyl)-2,2′,2″-nitrilotriethanol; DTT, dithiothreitol; FOM, figure of merit; GFOR, glucose-fructose oxidoreductase; MME, monomethyl ether; PEG, polyethylene glycol; SAD, single-wavelength anomalous dispersion; SDR, short-chain dehydrogenase/reductase; Se-Met, selenomethionine.

10.1021/bi052589q CCC: $33.50
Published on Web 08/01/2006

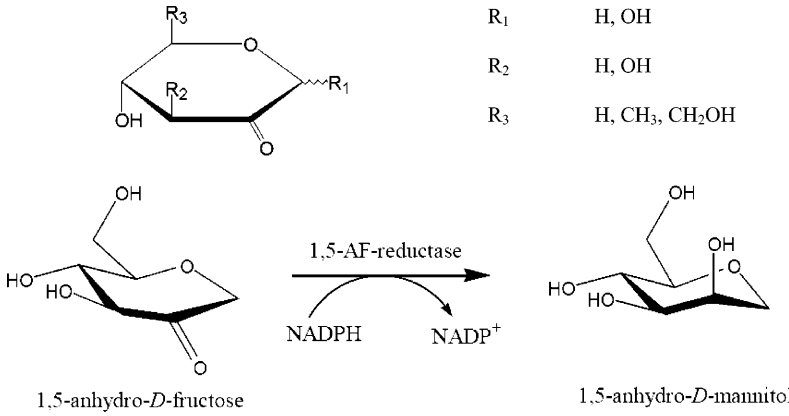

FIGURE 1: General structure of substrates and catalyzed reaction of 1,5-AF reductase (AFR) from *S. morelense*. 1,5-AF lacks the hydroxyl group at the C1 position and hence is not a hemiacetal but a cyclic ether. 1,5-AF is reduced by AFR to 1,5-AM under consumption of NADPH.

mammals (*11*, *12*), procedures for their chemical and biocatalytic synthesis have been developed (*1*, *13*, *14*). In this context, a microbial screening for new 1,5-AF-converting enzymes was performed which led to the bacterium *Sinorhizobium morelense* S-30.7.5 producing a new 1,5-anhydro-D-fructose reductase (AFR) with a unique substrate specificity and stereospecificity (Figure 1) (*14*). This AFR from *S. morelense* S-30.7.5 was characterized as a strictly NADPH-dependent monomeric enzyme of 35.1 kDa catalyzing the stereoselective reduction of 1,5-AF to 1,5-anydro-D-mannitol (1,5-AM) and of a number of 2-keto aldoses (osones) to the corresponding manno-configured aldoses (*14*). The AFR gene was cloned from *S. morelense* S-30.7.5, and on the basis of the derived polypeptide sequence of 333 amino acid residues, AFR was assigned to the GFO/IDH/MocA family (*14*). It was also shown that *S. morelense* S-30.7.5 AFR was distinct from hepatic AFR (*2*) with respect to the peptide sequence and stereoselectivity of 1,5-AF reduction (*14*). On the basis of the specificity and high stereoselectivity of AFR from *S. morelense* S-30.7.5, its applicability in the synthesis of 1,5-AM and related derivatives as well as for enzymatic analysis of 1,5-AF was demonstrated (*14*).

To provide insight into the fold of this new NADPH-dependent reductase, its cofactor and substrate specificity, and the mechanism of the catalyzed reaction, we undertook a crystallographic study of AFR from *S. morelense* S-30.7.5. Here we report the crystal structure and the analysis of AFR in complex with the oxidized cofactor $NADP^+$. Possible residues responsible for cofactor specificity, substrate binding, and catalysis are described. The results are presented in the context of homologous proteins and established mechanisms. The biotechnological potential of a constructed AFR variant (A13G) with dual cosubstrate specificity was demonstrated in an effective stereoselective conversion of 1,5-AF to 1,5-AM, using the cofactor NADH.

MATERIALS AND METHODS

Crystallization and Data Collection. Recombinant full-length 1,5-AF reductase (AFR) from *S. morelense* was produced in *E. coli* BL21(DE3) using pET-24a(+) as the expression vector and purified to homogeneity from crude bacterial extracts (*14*). Similarly, selenomethionine (Se-Met)-substituted AFR was expressed in *E. coli* B834(DE3) (Novagen) (*15*) using LeMaster medium supplemented with L-Se-Met (10 mg/mL) for growth and enzyme production (*16*). Selenomethionyl AFR was purified like native AFR (*14*) but under reducing conditions in the presence of 2 mM DTT. In crystallization trials, 20 mM DTT was used. Single crystals of AFR were obtained by performing hanging drop vapor diffusion experiments. For setting up the crystallization drops, equal volumes (each 1 μL) of reservoir solution [100 mM trisodium citrate (pH 5.6), 200 mM ammonium acetate, and 30% (w/v) PEG5000 MME] and protein solution [20 mg/mL AFR, 20 mM Bistris-HCl (pH 7.0), and 1 mM NADPH] were mixed on a cover slide and incubated over 500 μL of reservoir solution. Small crystals of AFR appeared after 3 days at 18 °C with dimensions of 250 μm $\times$ 80 μm $\times$ 80 μm. For Se-Met-substituted AFR, 10 mM DTT was added to the reservoir to keep the setup under reductive conditions. Protein crystals with Se-Met substitution appeared after 2 months with a morphology similar to that of the wild-type crystals. For X-ray experiments, the crystals were transferred into a cryo solution [100 mM trisodium citrate (pH 5.6), 200 mM ammonium acetate, 30% (w/v) PEG5000 MME, 7% (v/v) glycerol, and 2 mM DTT], mounted in nylon loops, and flash-frozen in liquid nitrogen. The space group was identified as $P2_1$. For the determination of the oxidation state of the cofactor NADP(H) in the crystals, UV−vis and fluorescence spectra of the crystals (before and after X-ray exposure) were collected (data not shown).

Structure Determination, Refinement, and Analysis. For phasing, a single-wavelength anomalous dispersion (SAD) data set at the Se peak wavelength (λ = 0.9788 Å) was collected at beam line X06SA (Swiss Light Source, Paul Scherrer Institut, Villigen, Switzerland). Data were processed and scaled using *MOSFLM* and *SCALA* as implemented in the *CCP4* program suite (*17*). AFR contains nine methionine sites per molecule, including the methionine in the N-terminal position. Analysis based on the Matthews coefficient (*18*) was ambiguous and indicated five to eight molecules per asymmetric unit. Therefore, the search for the selenium positions was carried out with different numbers of anomalous sites with *SHELXD* (*19*) in graphical user interface *HKL2MAP* (*20*). The solutions were judged by the correlation coefficient and were taken to be a good solution if the correlation coefficient was double that of the wrong solutions of the same run. The correct enantiomer of the heavy atom

sites could be distinguished by comparing the connectivity and contrast value after a first round of density modification and refinement of the heavy atom sites using *SHELXE* (*21*). Phasing of the anomalous data was performed with *SHARP/autoSHARP* (*22*) using the previously refined Se sites from *SHELXE*. An initial model was built using the auto build function of *RESOLVE* (*23*, *24*). In the model generated by *RESOLVE*, six molecules of AFR could be identified per asymmetric unit. The initial model could be further interpreted and completed by hand with the aid of the homologous protein structure of glucose-fructose oxidoreductase from *Zymomonas mobilis* [GFOR; PDB entry 1OFG (*25*)]. After several rounds of model building using *O* (*26*) and simulated annealing and energy minimization using *CNS* (*27*), R_{work} dropped to 26.9% and R_{free} to 29.3%.

A high-resolution native data set was collected at beamline ID14-2 (ESRF, Grenoble, France) and processed with *XDS* and *XSCALE* (*28*). Since the native crystals were isomorphous to those of the Se-Met-substituted protein, the refined model of the Se-Met-substituted protein was taken as a starting model for further refinement. The cofactor $NADP^+$ could be clearly located in the electron density map and was added to the model. A dictionary file of the cofactor was created by the *PRODRG* server (*29*). Further refinement was carried out with *REFMAC5* (*17*); model building was performed with *O* (*26*). After the value for R_{work} dropped to 23% and R_{free} to 27%, water molecules were added using *ARP/wARP* (*30*), and the suggested positions were manually verified with *O*. Full statistics for data collection and refinement are given in Table 1. The quality of the final structure was evaluated with *PROCHECK* (*31*). The analysis of the secondary structure composition was performed with *DSSP* (*32*). Fold-similarity searches were performed with *DALIlite* (*33*). All visualization and image production was performed with *PyMOL* (*34*).

Site-Directed Mutagenesis of the AFR Gene. Plasmid pPS18 containing the AFR gene (*14*) served as a template for mutagenesis using the QuickChange site-directed mutagenesis kit (Stratagene). PCR amplification was performed according to the manufacturer's instructions. The amplified DNA sequences were cloned into *E. coli* TOP10 (Qiagen) for DNA sequencing and then subcloned into expression vector pET-24a(+) as described recently (*14*).

Multiple-angle light scattering (MALS) was used to determine the oligomerization state of AFR. The analysis was performed with the Eclipse system (Wyatt Technology) consisting of an asymmetric flow field flow fractionation (AFFF) device connected to a miniDAWN multi-angle light scattering (MALS) unit with an in-line Shodex RI-101 refractive index detector. The miniDAWN was calibrated according to the manufacturer's instructions, and bovine serum albumin was used as a standard to evaluate the accuracy of the system. All measurements were taken in 20 mM Bistris-HCL (pH 7.2) and 150 mM NaCl at 20 °C. For separation, 87 μg of protein was injected into the AFFF channel (1 mL/min channel flow and 3 mL/min cross-flow) equipped with a 350 μm spacer and an ultrafiltration cellulose membrane (10K cutoff). The average molecular weight was determined by the Zimm plot method as implemented in the *ASTRA V* software package (Wyatt Technology).

Table 1: X-ray Data Collection, Phasing, and Refinement Statistics

	native	Se-Met
data and phasing statistics		
beamline	ESRF ID14-2	SLS X06SA
temperature (K)	100	100
wavelength (Å)	0.9771	0.9788
space group	$P2_1$	$P2_1$
unit cell parameters		
a (Å)	96.9	97.2
b (Å)	84.7	86.4
c (Å)	150.4	153.3
β (deg)	96.1	96.9
resolution range (Å)	20−2.2	20−2.6
highest-resolution shell (Å)	2.3−2.2	2.7−2.6
no. of unique reflections	118884	77758
completeness (%)[a]	96.6 (89.8)	99.6 (100)
redundancy	9.8	3.8
R_{sym} (%)[a,b]	7.7 (40.2)	9.2 (44.5)
$\langle I/\sigma(I)\rangle$[a]	10.8 (3.3)	11.3 (3.3)
Wilson *B* factor (Å^2)	39.8	44.4
phasing power (before DM)		0.915
FOM acentric/centric (before DM)		0.27/0.10
refinement statistics		
R_{work}/R_{free} value (%)[c,d]	19.0/25.1	26.9/29.3
Ramachandran plot (%)[e]		
most favored region	88.0	
allowed regions	10.0	
generously allowed regions	0.4	
estimated overall coordinate error[f]		
based on R_{free} (Å)	0.210	
based on maximum likelihood (Å)	0.167	
rms deviations from ideal values		
bonds (Å)	0.014	
angles (deg)	1.63	
average *B* factors (Å^2)		
protein (14 736 atoms)	40.6	
$NADP^+$ (288 atoms)	35.8	
acetate (24 atoms)	48.4	
water molecules (1305 molecules)	43.4	

[a] Values in parentheses are for the high-resolution bin. [b] $R_{sym} = 100\sum_h\sum_i|I_i(h) - \langle I_i(h)\rangle|/\sum_h\sum_i I_i(h)$, where $I_i(h)$ is the *i*th measurement and $\langle I_i(h)\rangle$ is the mean of all measurements of $I(h)$ for Miller indices *h*. [c] $R = \sum(||F_{obs}| - k|F_{calc}||)/\sum|F_{obs}|$, where F_{obs} and F_{calc} are observed and calculated structure factor amplitudes, respectively. [d] The R_{free} value is the *R* value obtained for a test set of reflections, consisting of a randomly selected 10% subset of the diffraction data not used during refinement (*77*). [e] Calculated using *PROCHECK* (*31*). [f] Calculated using *REFMAC5*.

RESULTS

Quality of the Model. The crystal structure of the bacterial 1,5-anhydro-D-fructose reductase (AFR) in complex with the cofactor $NADP^+$ has been determined at 2.2 Å resolution. The structure was determined by single-wavelength anomalous diffraction from Se-Met-labeled protein and refined against a native data set in the resolution range of 20.0−2.2 Å, resulting in crystallographic *R* factors of 19.0% (working set) and 25.1% (free set) with a good geometry according to the Ramachandran plot (*35*). The final model includes amino acid residues 2−333 in each monomer of the enzyme and contains six protein molecules and 1305 water molecules in the asymmetric unit (V_M = 3.0 Å^3/Da). Each monomer has one cofactor molecule $NADP^+$ and one acetate ion bound. Since UV−vis and fluorescence spectroscopy revealed no detectable amounts of the reduced form of the cofactor NADPH, almost complete oxidation of the cofactor within the crystals is assumed. The average crystallographic temperature factor (*B* factor) is 40.6 Å^2 for the six monomers.

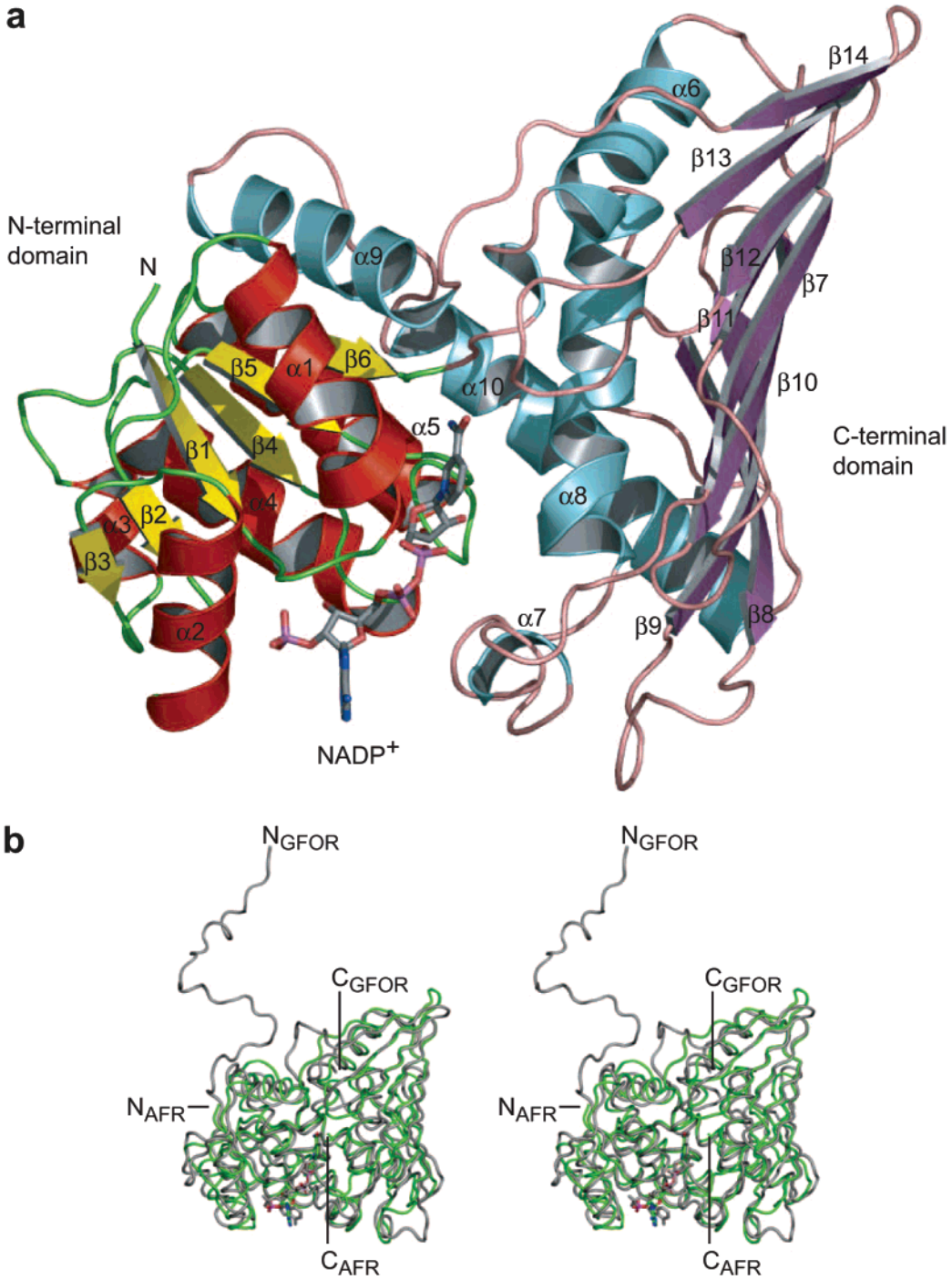

FIGURE 2: Secondary structure ribbon model of the AFR structure. (a) AFR consists of two structural domains. The N-terminal domain (α-helices colored red and *β*-strands yellow) has the architecture of a Rossmann fold. The dinucleotide $NADP^+$ (shown in stick representation) is bound between the N-terminal and C-terminal domain (α-helices colored cyan and *β*-strands magenta). (b) Stereo representation of the Cα trace of AFR (green) superimposed onto the structure of GFOR (gray). The dinucleotide $NADP^+$ is shown in stick representation.

The statistics for data collection and refinement are summarized in Table 1.

Overall Fold. AFR was crystallized in the presence of oxidized cofactor $NADP^+$ in space group $P2_1$ with six molecules per asymmetric unit. The structural analysis of the six monomers within the asymmetric unit revealed root-mean-square (rms) deviations of ~0.4 Å for monomers B−F compared with monomer A. This indicates that the monomers within the asymmetric unit are virtually identical. If not stated differently, only molecule A will be discussed further. The enzyme consists of two structural domains (Figure 2) with the binding pocket for the dinucleotide cofactor NADP(H) located between the two domains in a deep cleft. The N-terminal domain (residues 2−120) displays a typical α/*β* dinucleotide binding motif, the so-called Rossmann fold (*36*). It consists of a central *β*-sheet surrounded by six α-helices, of which one helix is contributed by the C-terminal domain. The larger C-terminal domain (residues 121−333) also possesses α/*β* topology and exhibits structural homology with members of the family of glyceraldehyde-3-phosphate dehydrogenase-like proteins in the SCOP database (*37*). A fold-similarity search with *DALI* (*38*) for homologous structures in the Protein Data Bank (*39*) revealed the nearest structural similarities of AFR with glucose-fructose oxidoreductase

Table 2: Results of the Structural Similarity Search Using the DALI Server

PDB entry	*Z* score	LALI[a]	rmsd[b]	% IDE[c]	ref
1OFG	38.7	327	2.2	24	*25*
1TLT	30.9	291	2.5	16	*78*
1GCU	25.1	267	2.8	14	*79*
1DPG	19.4	293	3.8	12	*49*

[a] Total number of equivalent residues. [b] Positional root-mean-square deviation of superimposed Cα atoms (in angstroms). [c] Percentage of sequence identity over equivalent positions.

from *Z. mobilis* (GFOR; PDB entry 1OFG). The best results of the *DALI* search are summarized in Table 2. Since the alignment with *ClustalW* (*40*) or *T-Coffee* (*41*) for these enzymes was error-prone, especially in the C-terminal region, a structure-based sequence alignment with *SEQUOIA* (*42*) was performed (Figure 3). Despite the high *Z* score, the number of conserved residues within these enzymes is remarkably low, and especially the C-terminal domain is lacking conserved residues within the compared enzymes (Figure 3).

N-Terminal Dinucleotide Binding Domain. Although the Rossmann fold is a quite common motif in the group of NAD(H)/NADP(H) binding proteins, their amino acid sequences are very diverse. Nevertheless, a so-called fingerprint region could be determined which is conserved within proteins displaying the architecture of the Rossmann fold (*43*, *44*). This region is approximately 30−35 residues long and includes β-strands β1 and β2 and connecting helix α1. In AFR, this region is formed by residues 3−33 (Figure 4). The central motif of the fingerprint region is a glycine-rich region between β-strand β1 and α-helix α1 with a GxGxxG consensus sequence for NAD(H) binding proteins (*43*). A low degree of sequence identity between dinucleotide binding proteins led to an extension of the consensus sequence for different protein families. For example, Jornvall et al. (*45*) postulated GxxxGxG as a consensus sequence for members of the short-chain dehydrogenase/reductase protein family and Hanukoglu et al. (*46*) a GxGxxA motif for NADP(H) binding proteins. The first and second glycine residues of these sequence motifs are located at the beginning and end of the loop between β-strand β1 and helix α1. The first glycine is important for a tight turn of the loop between β-strand β1 and helix α1. In AFR, the torsion angles are in a region ($\varphi = 130°$ and $\psi = 135°$) which cannot be achieved with amino acids other than glycine. The third glycine or the alanine in the case of NADP(H) binding proteins is located in the first turn of helix α1 and is directed toward the β-sheet. In AFR, the 8-GASTIA sequence is found in this region (Figures 3 and 4a,b). Just the first glycine residue is conserved. Instead of the second glycine, a serine residue is found at position 10 in AFR, whereas Ala13 is conserved in NADP(H) binding enzymes.

For NAD(H) binding proteins, Bellamancia et al. (*43*) and Kleiger and Eisenberg (*47*) described the necessity of small hydrophobic residues at the contact area between helix α1 and the central β-sheet which allows a close contact between α-helix and β-sheet. In AFR, this contact area is formed by large hydrophobic residues (Trp4, Leu6, Val17, and Ile21) (Figure 4a), which might prevent in combination with Ala13 a close contact between helix α1 and the central β-sheet. Helix α1 displays a kink after the second turn, which is also found in structurally homologous proteins such as GFOR (*25*), aspartate-β-semialdehyde dehydrogenase (*48*), and glucose-6-phosphate dehydrogenase (*49*). In these enzymes, a proline residue in the third turn interrupts the hydrogen bond network of the helix and enables an insertion of an amino acid into the second turn of the helix. In AFR, Gly19 is found in a position analogous to that of the proline residue (Figure 4a), causing the insertion of an amino acid residue in the second turn. This kink might have influence on the dipole moment of helix α1 and, therefore, might be important for cofactor binding.

C-Terminal Domain. One characteristic feature of the C-terminal domain is the large, mostly antiparallel oriented eight-stranded β−sheet, which terminates AFR at one side (Figure 2a). Besides this β-sheet, five helices belong to this domain. Helices α8 and α10 are located in the deep cleft between the two domains and participate on one hand in cofactor and substrate binding, and on the other hand, they accommodate amino acid residues which might contribute to the active site of substrate conversion. Helix α6 interacts with the C-terminal β-sheet, while α9, as described above, completes the Rossmann fold by binding to the β-sheet of the N-terminal domain. The large C-terminal β-sheet is on the inside mainly hydrophobic, whereas large hydrophilic and charged residues such as arginine or glutamate are located on the outside. In the crystal packing, a major contact between two AFR molecules is achieved by this β-sheet in such a manner that six AFR monomers in the asymmetric unit are arranged as three dimers (Figure 5). This crystal contact covers 1800 Å^2 of the monomer surface according to the definition of Lee and Richards (*50*). Structurally related enzymes are monomeric, like biliverdin-IXα reductase (*51*), but are also arranged in an oligomeric state like the dimeric glucose-6-phosphate dehydrogenase (*49*) and the tetrameric GFOR (*25*). The contacts within these oligomers are constituted by the C-terminal β-sheet similar to the crystal contact observed for ARF. However, the analysis of the oligomerization state of AFR was not conclusive. Whereas gel filtration chromatography clearly indicated the elution of AFR as a monomer, multiple-angle light scattering (MALS) experiments revealed the presence of a dimer in solution (data not shown).

For the long-chain dehydrogenases, C-terminal glycine-rich motifs (-GxGxxG- or -GxGxxGxxxG/A-) are described as being important for cofactor binding (*47*). To analyze the glycine-rich 204-GxGxxGxxxG sequence in the C-terminal moiety of AFR for potential cofactor or substrate binding, the G206I mutant was characterized. Since no kinetic effects for AFR(G206I) could be observed (Table 3), this motif seems not to be crucial for cofactor or substrate binding. This is in agreement with the position of this sequence in loop L15 far from the substrate binding site (Figures 2 and 3).

Nucleotide Binding Pocket. Electron density between the N-terminal domain and the C-terminal domain could clearly be assigned to the cofactor NADP(H) (Figure 6a). Since the reduced cofactor NADPH generally is unstable under aerobic and acidic conditions as used for crystallization of AFR, the question of whether the bound cofactor was still reduced or oxidized during crystallization arose. On the basis of the electron density distribution, a differentiation between the reduced and oxidized form was not possible. In solution, the

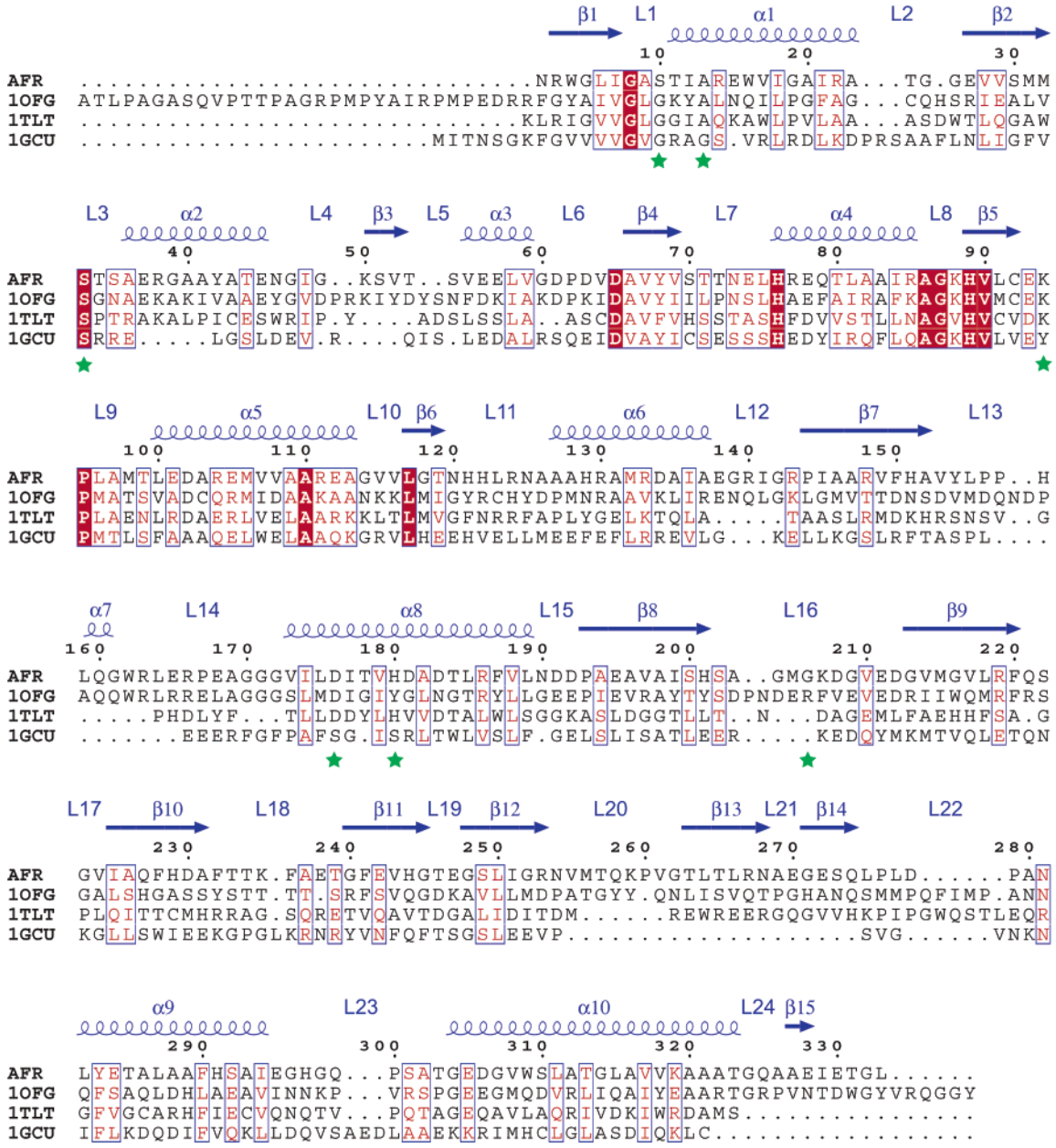

FIGURE 3: Sequence alignment of AFR with glucose-fructose oxidoreductase from *Z. mobilis* (1OFG) (*25*), a potential oxidoreductase from *E. coli* (1TLT) (*78*), and biliverdin-IXα reductase from rat (1GCU) (*79*). These three enzymes gave the highest score for the analysis of structural similarity with *DALI* (Table 2). The structure-based sequence alignment was performed with *SEQUOIA* (*42*). The figure was prepared with *ESPript* (*80*) using a similarity score of '0.7 0.5 I'. Color code for text and background: white letters boxed with red background for residues that are identical in all four proteins and red letters for similar residues. The secondary structure elements of AFR are depicted above the sequence alignment (arrows indicate *β*-strands and helices α-helices). Green stars mark the mutated positions: S10D, A13G, S33D, K94G, D176A, H180A, and G206I.

oxidation state of the cofactor can be determined by UV−vis absorption and fluorescence measurements. Washed and dissolved crystals did not exhibit the NAD(P)H characteristic absorption at 340 nm. Since fluorescence measurements are more sensitive [NAD(P)H exhibits significant fluorescence at 440 nm when excited at 325 nm, whereas the oxidized form, $NAD(P)^+$, does not], for further evaluation we performed fluorescence measurements within the protein crystals using a newly designed fluorescence spectrometer (*52*). Basically no fluorescence at 440 nm of the crystal (data not shown) indicated that the cofactor was mainly oxidized during crystallization, and the electron density distribution has to be interpreted as $NADP^+$. The cofactor is bound in a stretched manner in a deep cleft between the domains. The adenine ring and the nicotinamide ring are in an anti position according to their glycosidic bond. In addition, further undefined electron density could be assigned to one molecule of acetate per AFR active site. The acetate ion is bound in a pocket, which hosts most likely the active site, since residues Lys94, Asp176, and His180, which might participate in catalysis (see below), are surrounding this pocket. The environment of the adenine is surprisingly different between the GFOR−$NADP^+$ and AFR−$NADP^+$ complexes (Figures 6a−c and 7). Due to differences in the main-chain conformation and in sequence within loop region L4, the adenine rings adopt different orientations. Whereas the 2′-phosphate is bound in a similar pocket of the two proteins formed by AFR residues Ala9, Ser33, Thr34, and Arg38 (Ser116, Gly117,

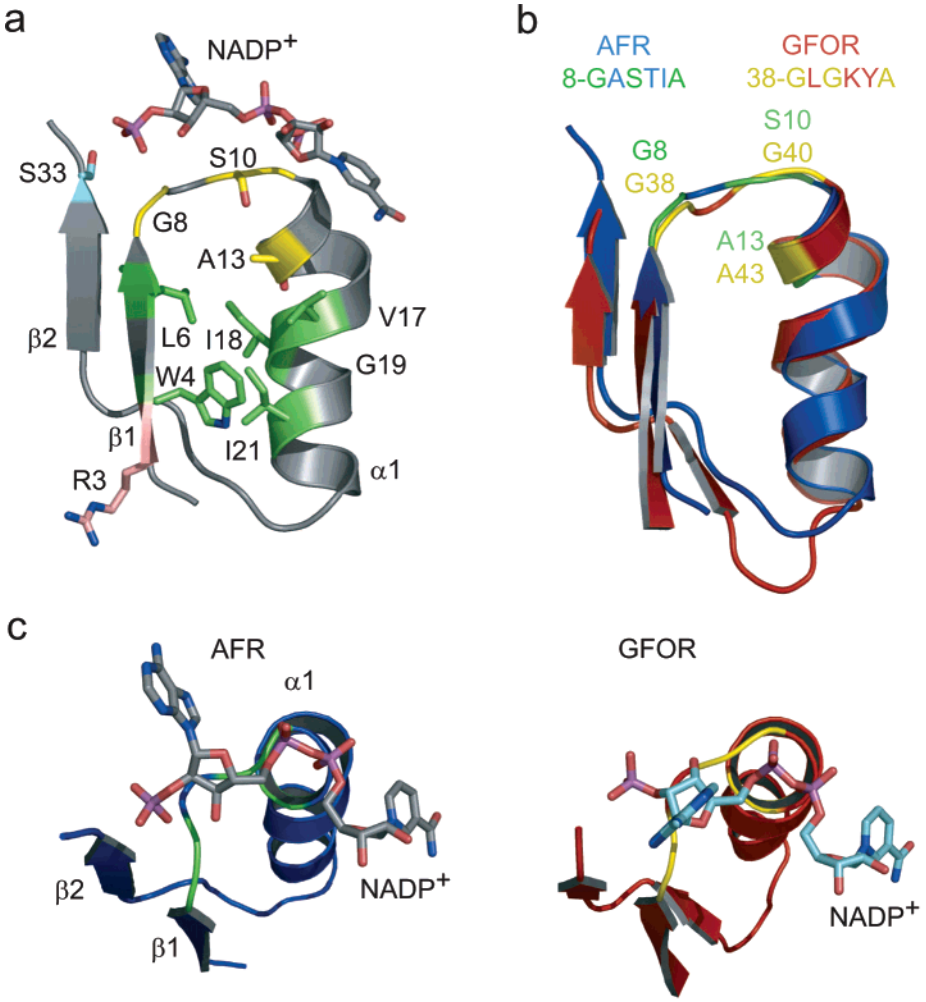

FIGURE 4: Structural alignment of the fingerprint region of AFR and GFOR. (a) The central motif of the fingerprint region is the loop between β-strand β1 and helix α1 (yellow). The contact area between the central β-sheet and helix α1 is colored green. Ser33 interacts with the 2′-phosphate group and is responsible for the coenzyme specificity. Arg3 forms a salt bridge with the conserved Asp65 at the beginning of β-strand β4 and is responsible for the stability of the fingerprint region. (b) Superposition of the fingerprint region of AFR and GFOR. The main chain has nearly the same conformation in both enzymes. (c) Stabilization of the pyrophosphate moiety by the dipole moment of helix α1. The conformation of the adenine moiety of the bound cofactor differs in both enzymes.

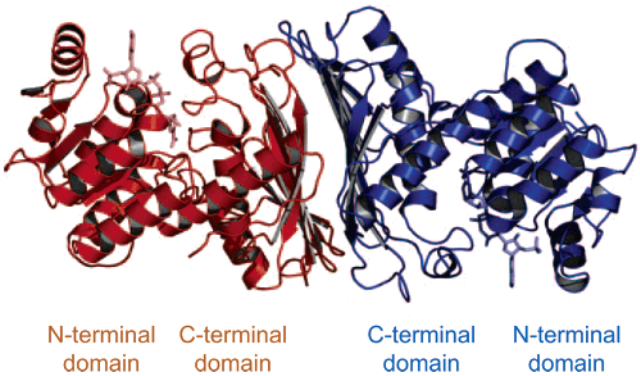

FIGURE 5: Crystal contact between two AFR monomers. The contact is made via the large C-terminal β-sheet. The covered area is 1800 Å^2, which corresponds to approximately 13% of the total surface of AFR. The cofactor NADP$^+$ is represented as sticks.

Lys121, and Tyr139 in GFOR, respectively), the adenine ring in the AFR complex is forced into a different orientation due to a cation$-\pi$ interaction with the guanidinium moiety of Arg38 in parallel geometry (*53*) (Figures 6b and 7, respectively).

An important region for the cofactor specificity and the preference of AFR for the phosphorylated cofactor NADPH is the region around the phosphate at the 2′-position of the adenine ribose. On one hand, this phosphate is a bulky group which needs space, which is provided by the action of Ala13 as described above. On the other hand, the negative charge, generated by this phosphate moiety, has to be compensated by the enzyme. The 2′-phosphate group fits in a binding pocket and interacts beside the peptide bond nitrogen of Ala9 with the side chains of Ser33, Thr34, and Arg38 (Figures 6b and 7, respectively)

The negative charge of the pyrophosphate bridge of the cofactor is stabilized by the positively charged N-terminus of the helix α1 dipole (Figure 4c,d), as previously described for proteins with Rossmann folds (*43*). On the opposite side, the pyrophosphate group binds to a loop between β-strand β7 and helix α7 of the C-terminal subunit. This loop covers the binding pocket and might prevent an easy diffusion of the cofactor from AFR. Therefore, a conformational change needed for cofactor binding can be proposed.

The nicotinamide and the connected ribose are positioned in a pocket between the N-terminal and C-terminal domains

Table 3: Kinetic Properties of AFR Variants[a]

	K_m (mM)				k_{cat} (s^{-1})		k_{cat}/K_m (M^{-1} s^{-1})	
	1,5-AF_{NADPH}	1,5-AF_{NADH}	$NADPH_{1,5-AF}$	$NADH_{1,5-AF}$	1,5-AF_{NADPH}	1,5-AF_{NADH}	1,5-AF_{NADPH}	1,5-AF_{NADH}
wild $type_{native}$	8.3 ± 0.04	nd	0.1 ± 0.02	ND	216 ± 5	ND	26020	ND
wild $type_{rec}$	6.4 ± 0.01	nd	0.06 ± 0.01	ND	145 ± 13	ND	22650	ND
A13G	8.5 ± 0.02	11.1 ± 0.3	0.02 ± 0.01	1.1 ± 0.04	405 ± 6	12.4 ± 0.9	47650	1110
A13G/S10G	7.1 ± 0.05	39.0 ± 0.7	0.38 ± 0	1.2 ± 0.1	369 ± 5	5.5 ± 0.1	51970	140
A13G/S33D	20.2 ± 0.2	3.2 ± 0.5	1.0 ± 0	1.1 ± 0.05	6.3 ± 0.8	13.5 ± 0.7	310	4210
S10G	3.5 ± 0.1	nd	0.27 ± 0.1	ND	119 ± 9	ND	34000	ND
S33D	nd	nd	ND	ND	ND	ND	ND	ND
K94G	22.5 ± 1.5	nd	0.2 ± 0.05	ND	4.2 ± 0.2	ND	190	ND
D176A	49.0 ± 1	nd	ND	ND	1.3 ± 0.1	ND	26	ND
H180A	8.9 ± 0.4	nd	ND	ND	3.7 ± 0.1	ND	420	ND
G206I	8.3 ± 0.02	nd	0.06 ± 0.01	ND	156 ± 1	ND	18790	ND

[a] ND, not determined; nd, not detectable. k_{cat}/K_m values were calculated from the means of the respective K_m and k_{cat} values. Enzyme activities were measured in the spectrophotometric assay for AFR (*14*) using an optimal buffer and pH for each variant. Usually, 100 mM Bistris-HCl (pH 6.5) was used except for D176A and H180A which were assayed in Tris-HCl at pH 7.5 and 8.0, respectively. If the 1,5-AF concentration was varied for K_m determinations, the NAD(P)H concentration (index) was kept constant at 0.28 mM. If the NAD(P)H concentration was varied, the 1,5-AF concentration (index) was kept constant at 30 or 100 mM, where appropriate (*14*).

(Figure 2). Ribose binding is mediated by hydrogen bonding to a loop between β-strand β5 and helix α5. This loop includes the functional motif 93-EKP (*25*), which is part of the 86-AGKHVxCEKP motif and conserved in the class of sugar dehydrogenases (*54*). The side-chain carboxylate of Glu93 makes a hydrogen bond to the carboxy amide group of the nicotinamide ring. Furthermore, the side chain is in close contact (2.7 Å) with the NC2 atom of the nicotinamide ring, making a C−H···O hydrogen bond feasible (*55*−*57*). Similar C−H···O hydrogen bonds around the nicotinamide ring were observed for other NAD(P)H-dependent proteins (SCOR enzyme family) and are discussed as being important for cofactor binding (*58*). Whereas the main-chain carbonyl group of Lys94 performs hydrogen bonding to the 2′- and 3′-OH groups of the nicotinamide ribose, the NZ atom of Lys94 is close (5 Å) to the nicotinamide ring forming a cation−π interaction (*53*). In addition, Lys94 might be involved in substrate binding as described below. The peptide bond between Lys94 and Pro95 adopts the cis conformation and might be an important factor for the correct binding mode of the nicotinamide ring and the substrate during the enzymatic reaction, as been described for the homologous residue, Pro149, in glucose-6-phosphate dehydrogenase (*59*). An additional hydrogen bond with the 3′-OH group of the ribose is made by His76, which is conserved in the GFO/IDH/MocA protein family (*60*, *61*).

To elucidate the similarity of AFR with GFOR and to change the cofactor specificity of the strictly NADPH-dependent enzyme to utilize NADH as well, different site-directed mutations were analyzed (S10G, A13G, S33D, S10G/A13G, and A13G/S33D). The AFR(A13G) enzyme exhibited dual cofactor specificity and could utilize either NADPH or NADH (Table 3 and Figure 8). However, the K_m for NADH was ∼2 orders of magnitude higher than that for NADPH. Amino acid Ser33 is positioned at the C-terminal end of β-strand β2 and is part of the fingerprint motif. In NAD(H)-dependent enzymes, this position is occupied by amino acids with a negatively charged side chain (*43*) which forms hydrogen bonds with the 2′-hydroxy group of the adenine ribose moiety of NAD(H). An acidic residue at this position in AFR would form repulsive interactions with the 2′-phosphate group of NADPH. Whereas the mutation of the respective residue in GFOR caused the loss for NADP(H) dependency and acceptance of NAD(H) as a cofactor (*54*), the analogous S33D mutation for AFR resulted in an inactive enzyme. No reducing activity toward 1,5-AF and two other 2-keto aldoses as substrates could be observed (*62*). This indicates that neither NADP(H) nor NAD(H) can be bound any longer. This difference in the behavior between AFR and GFOR is probably caused by the changed mode of binding of the 2′-phosphate ribose adenine moiety (Figure 6).

Active Site. The catalyzed reaction of AFR is a hydride transfer from the nicotinamide ring of the cofactor to the substrate. Therefore, the active site is supposed to be in a solvent accessible pocket of the protein near the nicotinamide moiety of the cofactor. This pocket is located between the N-terminal domain and the C-terminal domain. A close-up view of this pocket is given in Figure 6b. In the crystal structure, an acetate ion, which was present in the crystallization buffer, is bound within this pocket. The acetate ion is directly coordinated or coordinated via hydrogen bonds mediated by water molecules to the side chains of Lys94, Arg163, Asp176, and His180. Since kinetic experiments performed in acetate buffer revealed a slower turnover of 1,5-AF compared to that of Bistris-HCl and Tris-HCl buffer (*14*), acetate might be a competitive inhibitor. Therefore, the observed acetate molecule provides some insight into the determinants of the binding pocket, and residues Lys94, Arg163, and Asp176 are probably involved in substrate binding as well. Since cocrystallization or soaking of crystals with 1,5-AF or substrate analogues was not successful, the K94G, D176A, and H180A mutations were used as a first probe for the active site. The replacement of Lys94 with a glycine did not change the binding affinity (K_m) for the cofactor but significantly increased the K_m value for the substrate, which was concomitant with a significant decrease in k_{cat} as well as the corresponding k_{cat}/K_m values (Table 3), suggesting that this residue is involved in the binding of the substrate and in the enzymatic reaction. Similar effects were observed for the D176A and H180A variants (Table 3), prompting us to propose that at least three residues, Lys94, Asp176, and His180, are involved in substrate binding and catalysis. In this context, His180 might serve as an acid−base catalyst in polarizing the carbonyl function of 1,5-AF

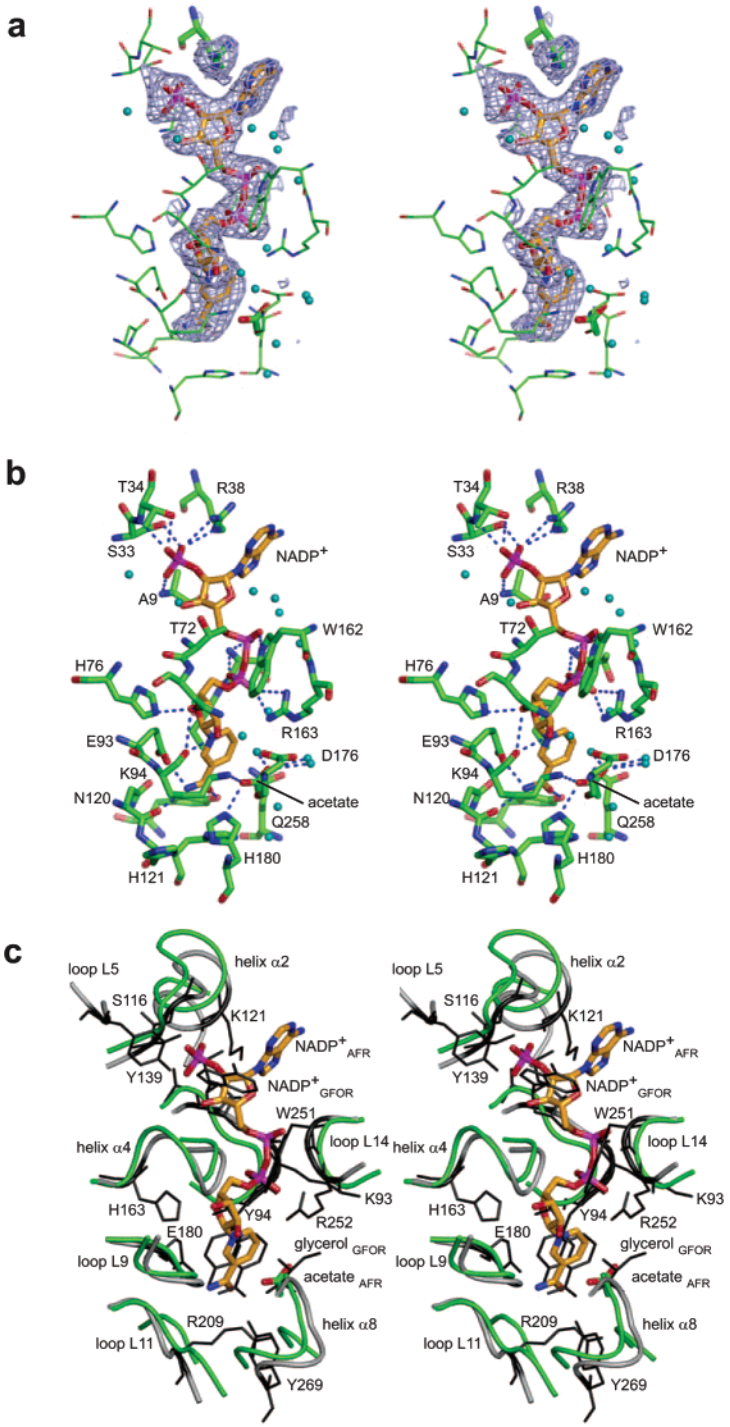

FIGURE 6: Binding cleft for the cofactor $NADP^+$ and the substrate. (a) Stereoview of the electron density map around $NADP^+$ together with parts of the final refined model. $|F_o| - |F_c|$ σ_a-weighted electron density omit map at the 2σ contour level obtained with the final structure at 2.2 Å resolution after removal of $NADP^+$ and the side chain of Arg38 and 10 subsequent cycles of restrained refinement with *REFMAC5*. All residues contacting $NADP^+$ are included and represented as sticks. (b) Stereoview of the $NADP^+$ binding and the acetate binding pocket of AFR. The carbon atoms of the cofactor are colored orange, and all other carbon atoms are colored green. Hydrogen bonds are represented as blue dashed lines. The nicotinamide ring is coordinated by the conserved 93-EKP motif. In the crystal structure at the putative active site pocket, an acetate ion is bound to Lys94, Arg163, and Asp176 directly or via water molecules. On the opposite side of the nicotinamide ring, His180 is believed to act as an acid−base catalyst. His121 and His122 are probably supporting the action of His180. (c) Stereoview and comparison of the $NADP^+$ binding pocket in AFR and GFOR. The $NADP^+$ and the bound acetate molecule of AFR are represented in sticks with bonds colored green. The main-chain traces of AFR protein regions contacting $NADP^+$ and acetate are represented as green loops. The $NADP^+$ and bound glycerol in the GFOR structure (PDB entry 1H6D) together with the interacting residues of GFOR are superimposed and represented with gray sticks. The main-chain traces of the contacting regions of GFOR are represented as dark gray loops. All residue numbers refer to GFOR. The adenine ring of AFR forms a cation$-\pi$ stacking interaction with the side chain of Arg38, whereas in GFOR, this orientation is not possible due to the presence of Tyr139 from loop L5. The active site of GFOR has important contributions from residues Arg209 and Tyr269. In AFR, this part of the active site is formed by residues His121, His122, and His180 (see panel b).

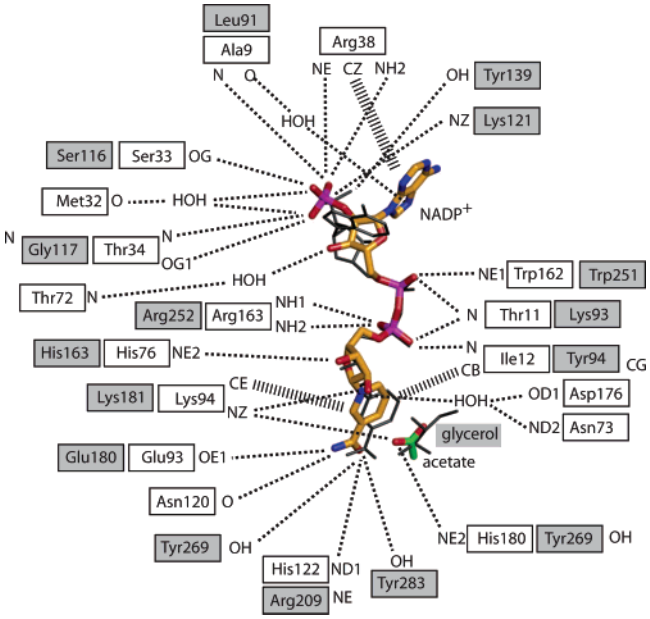

FIGURE 7: Schematic diagram of the $NADP^+$ binding site of AFR and GFOR. $NADP^+$ and bound acetate of AFR are given in stick representation. Atoms are shown in standard colors: orange ($NADP^+$) and green (acetate) for carbon, blue for nitrogen, red for oxygen, and magenta for phosphorus. The $NADP^+$ and glycerol molecule in the GFOR structure (PDB entry 1H6D) are superimposed and represented with black lines. Potential hydrogen bonds are indicated with thin dashed lines; stacking interactions are represented with thick dashed lines. Shaded boxes represent (equivalent) residues of GFOR.

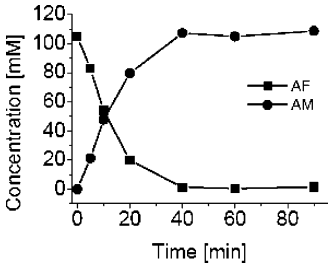

FIGURE 8: Conversion of 1,5-AF to 1,5-AM by AFR(A13G) using NADH as a cofactor. Values represent means of double determinations. The cofactor NADH was regenerated in situ through the oxidation of formic acid to carbon dioxide by formate dehydrogenase (FDH). The bioconversion was performed in a 50 mL Erlenmeyer flask with gentle stirring at 30 °C. The reaction mixture contained in a final volume of 8 mL the following reagents: 50 mM Bistris-HCl (pH 6.5), 29 units of AFR(A13G), 32 units of formate dehydrogenase (FDH, Roche), 105 mM 1,5-AF, 105 mM sodium formate, 0.6 mM NADH, and 2.5 mM NAD^+.

to enable the transfer of the hydride from NADPH to the substrate.

DISCUSSION

This is the first report on a crystal structure of an AFR enzyme. It shows that AFR from the bacterium *S. morelense* S-30.7.5 is composed of two domains. The N-terminal domain displays a Rossmann fold and is mainly responsible for the cofactor binding and its specificity. The C-terminal domain harbors the residues which are involved in substrate binding and catalysis. Apparently, there are no structural similarities between prokaryotic and eukaryotic AFR (*2*), as the latter is similar in sequence to members of the aldose reductase protein family possessing a TIM barrel as a typical structural element (*63*). Rather, a fold-similarity search revealed the closest structural match of *S. morelense* AFR with glucose-fructose oxidoreductase from *Z. mobilis* (GFOR; PDB entry 1OFG) (*54*).

The sequence and structural alignment revealed four conserved regions, which are important for binding of the cofactor NADP(H) and the carbohydrate substrate: β1−L1−α1 region, L3−α2−L4−β3−L5 region, β4−L7 region, and α4−L8−β5−L9 region. Within the β1−L1−α1 region, AFR displays with the 8-GASTIA residues the most significant difference in sequence for a characteristic glycine-rich loop GxGxxG (*43*).

The first glycine is important for a tight turn of the loop between β-strand β1 and helix α1. The second conserved glycine should allow, due to the missing side chain, a close contact between the protein backbone and the pyrophosphate unit of the dinucleotide cofactor. However, the structural alignment of AFR with GFOR and related proteins reveals that Ser10 has an only slight influence on the loop conformation (Figure 4b). The third glycine of the GxGxxG motif in NAD(H) binding proteins (*43*) is important for a close contact between helix α1 and the β-sheet of the Rossmann fold. In AFR, but also in other NADP(H) binding proteins such as glutathione reductase (*64*) or GFOR (*25*), this residue is substituted with an alanine (*46*). This substitution is believed to contribute together with the larger hydrophobic residues in the contact area between helix α1 and strand β1 to the widening of the cofactor binding pocket and to create more space for the additional bulky 2′-phosphate group (*65*). This interpretation is in agreement with kinetic characteristics of AFR(A13G) showing dual cofactor specificity.

A small uncharged residue at the end of β-strand β2 is needed to host the 2′-phosphate moiety in AFR (*43*). In contrast, NADH binding proteins possess an acidic residue at this position, which is believed to expel the phosphorylated cofactor in these enzymes (*66*). With respect to AFR, this effect could apply to the enzymatically inactive mutant S33D. However, for a change in cofactor specificity, a single mutation of Ser33 is not sufficient, indicating a synergistic effect with, for example, Ser10 and Ala13.

The comparison of the binding mode of the bound cofactor between AFR and GFOR revealed a different orientation of the ADP moiety (Figures 6c and 7). Loop L3 adopts a different conformation in GFOR, enabling Tyr139 of the larger loop L5 to interact with the 2′-phosphate group of $NADP^+$ in GFOR (Figure 6c). Due to differences in the sequence, conformation, and size of the corresponding loops in AFR compared to GFOR, similar interactions are not possible. Instead, the side chain of AFR residue Arg38 stabilizes the adenine ring in a different orientation.

AFR catalyzes the reduction of a carbonyl function to an alcohol function which implies the polarization of the carbonyl group for the hydride transfer. The mechanisms of such reactions are well established for metal-independent short-chain dehydrogenase/reductase (SDR) enzymes (*67*, *68*). In SDR enzymes, a tyrosine acts as an acid transferring the proton from its side-chain hydroxyl group to the carbonyl group of the substrate (*69*). Since a pK_a of ~10 of the tyrosine hydroxyl group is too high for it to act as an acid under physiological conditions, an adjacent base residue (arginine or lysine) and a substrate-stabilizing serine lower the pK_a and act as a catalytic triad (*70*). A tyrosine and a

basic amino acid residue are constituents of the active sites in GFOR and biliverdin-IXα reductase, which otherwise are structurally distinct from SDR (*25*, *51*). Nevertheless, the spatial orientation of these residues implies a similar mechanism postulated for malate dehydrogenase (MDH) and lactate dehydrogenase (LDH). In these enzymes, the catalytic base is a histidine residue acting with an aspartate residue as a proton relay system, thus polarizing the carbonyl function (*71*, *72*). With respect to AFR, both residues, His180 and Asp176, could be involved in catalysis as their substitutions caused significant decreases in k_{cat}. By spatial analogy to Tyr269 in GFOR (Figures 6b,c and 7) and to His240 in G6PD (*73*, *74*), which superimposes very well with His180, we propose His180 as the residue that acts as a general acid−base catalyst in AFR to facilitate the transfer of the hydride from NADPH to the carbonyl carbon of the substrate. His180 is close to acidic residue Asp176, but the distance of 5.9 Å makes a proton relay system similar to that of MDH and LDH unlikely. Nevertheless, the spatial arrangement around His180 leaves the possibility that other residues participate in the activation of the carbonyl group by His180. For example, His121 and His122 are close enough to His180 to enable the buildup of a hydrogen bonding cascade. However, it has to be considered that the active site of AFR might adopt a conformation with bound substrate subtly but significantly different from that observed in the presence of a bound acetate molecule. Furthermore, in GFOR and G6PD, a more drastic reduction in catalytic activity has been observed upon exchange of the proposed general acid−base catalyst, while in AFR, substitution of His180 had a weaker effect. Notably, the D176A substitution has an even greater impact on the k_{cat} decrease of AFR (~170-fold) which could arise in part from a conformation affecting the active site.

Biotechnological Importance of AFR. The elucidated structure of AFR provides a rational basis for improving the catalytic performance of this biocatalyst. Since 1,5-AF can be produced in bulk amounts from starch with α-(1,4)-glucan lyase, it has become an interesting synthon for various syntheses (*1*). The stereoselective reduction of 1,5-AF yields interesting cyclic polyols, of which at least 1,5-AM has the potential to influence type II diabetes beneficially (*7*, *10*). The biocatalytic synthesis with AFR yields enantiomerically pure 1,5-AM (*14*), in a degree of purity that cannot be achieved by chemical synthesis (*13*), irrespective of environmental concerns. As wild-type AFR strictly depends on NADPH, which is 10 times as expensive and much less stable than NADH (*75*, *76*), we were interested in changing the cosubstrate specificity of AFR by molecular techniques to make the process economically feasible. As a first result, we obtained two AFR variants (A13G and A13G/S33D) with dual cosubstrate specificity and promising catalytic efficiencies (k_{cat}/K_m) in the presence of NADH, albeit the k_{cat}/K_m for 1,5-AF of the A13G variant is still 40 times lower than that of wild-type AFR. Nevertheless, AFR(A13G) proved itself in a bioconversion of 100 mM 1,5-AF to 1,5-AM, as the reaction was complete within a short period of time. Since AFR also catalyzes the reduction of 2-keto aldoses (osones) to the corresponding manno-configured aldoses, a broader application of this enzyme in carbohydrate chemistry can be envisaged (*14*).

ACKNOWLEDGMENT

We are grateful to Ardina Grüber for analysis via MALDI mass spectrometry. We thank Björn Klink for assistance during data collection and for fluorescence spectroscopy and Markus Greiner and Carsten Burgard for MALS analysis. We thank the beamline staff of ID14 at ESRF and C. Schulze-Briese and T. Tomizaki for assistance at the Swiss Light Source for excellent technical support during data collection.

SUPPORTING INFORMATION AVAILABLE

Table of oligonucleotide primers used for site-directed mutagenesis. This material is available free of charge via the Internet at http://pubs.acs.org.

REFERENCES

1. Andersen, S. M., Lundt, I., Marcussen, J., and Yu, S. (2002) 1,5-Anhydro-D-fructose; a versatile chiral building block: Biochemistry and chemistry, *Carbohydr. Res. 337*, 873−890.
2. Sakuma, M., Kametani, S., and Akanuma, H. (1998) Purification and some properties of a hepatic NADPH-dependent reductase that specifically acts on 1,5-anhydro-D-fructose, *J. Biochem. 123*, 189−193.
3. Kametani, S., Shiga, Y., and Akanuma, H. (1996) Hepatic production of 1,5-anhydrofructose and 1,5-anhydroglucitol in rat by the third glycogenolytic pathway, *Eur. J. Biochem. 242*, 832−838.
4. Konishi, Y., Hashima, K., and Kishida, K. (2000) Increases in 1,5-anhydroglucitol levels in germinating amaranth seeds and in ripening banana, *Biosci., Biotechnol., Biochem. 64*, 2462−2465.
5. Shiga, Y., Mizuno, H., and Akanuma, H. (1993) Conditional synthesis and utilization of 1,5-anhydroglucitol in *Escherichia coli*, *J. Bacteriol. 175*, 7138−7141.
6. Shiga, Y., Kametani, S., Kadokura, T., and Akanuma, H. (1999) 1,5-Anhydroglucitol promotes glycogenolysis in *Escherichia coli*, *J. Biochem. 125*, 166−172.
7. Ahren, B., Holst, J. J., and Yu, S. (2000) 1,5-Anhydro-D-fructose increases glucose tolerance by increasing glucagon-like peptide-1 and insulin in mice, *Eur. J. Pharmacol. 397*, 219−225.
8. Yamanouchi, T., Inoue, T., Ichiyanagi, K., Sakai, T., and Ogata, N. (2003) 1,5-Anhydroglucitol stimulates insulin release in insulinoma cell lines, *Biochim. Biophys. Acta 1623*, 82−87.
9. Buse, J. B., Freeman, J. L., Edelman, S. V., Jovanovic, L., and McGill, J. B. (2003) Serum 1,5-anhydroglucitol (GlycoMark): A short-term glycemic marker, *Diabetes Technol. Ther. 5*, 355−363.
10. Ahren, B., and Yu, S. (2004) Use of a cyclic ether for the preparation of medicaments affecting glucose tolerance. U.S. Patent Appl. 20,020,198,158.
11. Yu, S., Mei, J., and Ahren, B. (2004) Basic toxicology and metabolism studies of 1,5-anhydro-D-fructose using bacteria, cultured mammalian cells, and rodents, *Food Chem. Toxicol. 42*, 1677−1686.
12. Tazawa, S., Yamato, T., Fujikura, H., Hiratochi, M., Itoh, F., Tomae, M., Takemura, Y., Maruyama, H., Sugiyama, T., Wakamatsu, A., Isogai, T., and Isaji, M. (2005) SLC5A9/SGLT4, a new Na^+-dependent glucose transporter, is an essential transporter for mannose, 1,5-anhydro-D-glucitol, and fructose, *Life Sci. 76*, 1039−1050.
13. Andersen, S. M., Lundt, I., and Marcussen, J. (2000) 1,5-Anhydro-D-fructose: Stereoselective conversion to 1,5-anhydroalditols and deoxy/amino substituted analogues, *J. Carbohydr. Chem. 19*, 717−725.
14. Kühn, A., Yu, S., and Giffhorn, F. (2006) Catabolism of 1,5-anhydro-D-fructose in *Sinorhizobium morelense* S-30.7.5: Discovery, characterization, and overexpression of a new 1,5-anhydro-D-fructose reductase and its application in sugar analysis and rare sugar synthesis, *Appl. Environ. Microbiol. 72*, 1248−1257.
15. Van Duyne, G. D., Standaert, R. F., Karplus, P. A., Schreiber, S. L., and Clardy, J. (1993) Atomic structures of the human immunophilin FKBP-12 complexes with FK506 and rapamycin, *J. Mol. Biol. 229*, 105−124.

16. Hendrickson, W. A., Horton, J. R., and LeMaster, D. M. (1990) Selenomethionyl proteins produced for analysis by multiwavelength anomalous diffraction (MAD): A vehicle for direct determination of three-dimensional structure, *EMBO J. 9*, 1665−1672.
17. Collaborative Computational Project Number 4 (1994) The CCP4 Suite: Programs for Protein Crystallography, *Acta Crystallogr. D50*, 760−763.
18. Matthews, B. W. (1968) Solvent content of protein crystals, *J. Mol. Biol. 33*, 491−497.
19. Schneider, T. R., and Sheldrick, G. M. (2002) Substructure solution with SHELXD, *Acta Crystallogr. D58*, 1772−1779.
20. Pape, T., and Schneider, T. R. (2004) HKL2MAP: A graphical user interface for phasing with SHELX programs, *J. Appl. Crystallogr. 37*, 843−844.
21. Sheldrick, G. M. (2002) Macromolecular phasing with SHELXE, *Z. Kristallogr. 217*, 644−650.
22. de La Fortelle, E., and Bricogne, G. (1997) Maximum-likelihood heavy-atom parameter refinement for multiple isomorphous replacement and multiwavelength anomalous diffraction methods, *Methods Enzymol. 276*, 472−494.
23. Terwilliger, T. (2003) Automated main-chain model building by template matching and iterative fragment extension, *Acta Crystallogr. D59*, 38−44.
24. Terwilliger, T. (2003) Automated side-chain model building and sequence assignment by template matching, *Acta Crystallogr. D59*, 45−49.
25. Kingston, R. L., Scopes, R. K., and Baker, E. N. (1996) The structure of glucose-fructose oxidoreductase from *Zymomonas mobilis*: An osmoprotective periplasmic enzyme containing non-dissociable NADP, *Structure 4*, 1413−1428.
26. Jones, T. A., Zou, J. Y., Cowan, S. W., and Kjeldgaard, M. (1991) Improved methods for building protein models in electron density maps and locations of errors in these models, *Acta Crystallogr. A47*, 110−119.
27. Brunger, A. T., Adams, P. D., Clore, G. M., Delano, W. L., Gros, P., Grossekunstleve, R. W., Jiang, J. S., Kuszewski, J., Nilges, M., Pannu, N. S., Read, R. J., Rice, L. M., Simonson, T., and Warren, G. L. (1998) Crystallography and NMR system: A new software suite for macromolecular structure determination, *Acta Crystallogr. D54*, 905−921.
28. Kabsch, W. (1993) Automatic processing of rotation diffraction data from crystals of initially unknown symmetry and cell constants, *J. Appl. Crystallogr. 26*, 795−800.
29. Schuttelkopf, A. W., and Van Aalten, D. M. (2004) PRODRG: A tool for high-throughput crystallography of protein−ligand complexes, *Acta Crystallogr. D60*, 1355−1363.
30. Morris, R. J., Perrakis, A., and Lamzin, V. S. (2003) ARP/wARP and Automatic Interpretation of Protein Electron Density Maps, *Methods Enzymol. 374*, 229−244.
31. Laskowski, R. A., MacArthur, M. W., Moss, D. S., and Thornton, J. M. (1993) Procheck: A Programm to Check the Stereochemical Quality of Protein Structures, *J. Appl. Crystallogr. 26*, 283.
32. Kabsch, W., and Sander, C. (1983) Dictionary of protein secondary structure. Pattern recognition of hydrogen bonded and geometrical features, *Biopolymers 22*, 2577−2637.
33. Holm, L., and Park, J. (2000) DaliLite workbench for protein structure comparison, *Bioinformatics 16*, 566−567.
34. Delano, W. L. (2004) *The PyMol molecular graphics system*, DeLano Scientific, LLC, San Carlos, CA.
35. Ramakrishnan, C., and Ramachandran, G. N. (1965) Stereochemical criteria for polypeptide and protein chain conformations. II. Allowed conformations for a pair of peptide units, *Biophys. J. 5*, 909−933.
36. Buehner, M., Ford, G. C., Moras, D., Olsen, K. W., and Rossman, M. G. (1974) Structure determination of crystalline lobster D-glyceraldehyde-3-phosphate dehydrogenase, *J. Mol. Biol. 82*, 563−585.
37. Murzin, A. G., Brenner, S. E., Hubbard, T., and Chothia, C. (1995) SCOP: A structural classification of proteins database for the investigation of sequences and structures, *J. Mol. Biol. 247*, 536−540.
38. Holm, L., and Sander, C. (1993) Protein structure comparison by alignment of distance matrices, *J. Mol. Biol. 233*, 123−138.
39. Berman, H. M., Westbrook, J., Feng, Z., Gilliland, G., Bhat, T. N., Weissig, H., Shindyalov, I. N., and Bourne, P. E. (2000) The Protein Data Bank, *Nucleic Acids Res. 28*, 235−242.
40. Thompson, J. D., Higgins, D. G., and Gibson, T. J. (1994) CLUSTAL W: Improving the sensitivity of progressive multiple sequence alignment through sequence weighting, position-specific gap penalties and weight matrix choice, *Nucleic Acids Res. 22*, 4673−4680.
41. Notredame, C., Higgins, D. G., and Heringa, J. (2000) T-Coffee: A novel method for fast and accurate multiple sequence alignment, *J. Mol. Biol. 302*, 205−217.
42. Bruns, C. M., Hubatsch, I., Ridderstrom, M., Mannervik, B., and Tainer, J. A. (1999) Human glutathione transferase A4-4 crystal structures and mutagenesis reveal the basis of high catalytic efficiency with toxic lipid peroxidation products, *J. Mol. Biol. 288*, 427−439.
43. Bellamacina, C. R. (1996) The nicotinamide dinucleotide binding motif: A comparison of nucleotide binding proteins, *FASEB J. 10*, 1257−1269.
44. Wierenga, R. K., Terpstra, P., and Hol, W. G. (1986) Prediction of the occurrence of the ADP-binding $\beta\alpha\beta$-fold in proteins, using an amino acid sequence fingerprint, *J. Mol. Biol. 187*, 101−107.
45. Jornvall, H., Persson, B., Krook, M., Atrian, S., Gonzalezduarte, R., Jeffery, J., and Ghosh, D. (1995) Short-Chain Dehydrogenases Reductases (Sdr), *Biochemistry 34*, 6003−6013.
46. Hanukoglu, I., and Gutfinger, T. (1989) cDNA sequence of adrenodoxin reductase. Identification of NADP-binding sites in oxidoreductases, *Eur. J. Biochem. 180*, 479−484.
47. Kleiger, G., and Eisenberg, D. (2002) GXXXG and GXXXA motifs stabilize FAD and NAD(P)-binding Rossmann folds through C(α)−H···O hydrogen bonds and van der Waals interactions, *J. Mol. Biol. 323*, 69−76.
48. Hadfield, A., Kryger, G., Ouyang, J., Petsko, G. A., Ringe, D., and Viola, R. (1999) Structure of aspartate-β-semialdehyde dehydrogenase from *Escherichia coli*, a key enzyme in the aspartate family of amino acid biosynthesis, *J. Mol. Biol. 289*, 991−1002.
49. Rowland, P., Basak, A. K., Gover, S., Levy, H. R., and Adams, M. J. (1994) The three-dimensional structure of glucose 6-phosphate dehydrogenase from *Leuconostoc mesenteroides* refined at 2.0 Å resolution, *Structure 2*, 1073−1087.
50. Lee, B., and Richards, F. M. (1971) The interpretation of protein structures: Estimation of static accessibility, *J. Mol. Biol. 55*, 379−400.
51. Whitby, F. G., Phillips, J. D., Hill, C. P., McCoubrey, W., and Maines, M. D. (2002) Crystal structure of a biliverdin IXα reductase enzyme-cofactor complex, *J. Mol. Biol. 319*, 1199−1210.
52. Klink, B. U., Goody, R. S., and Scheidig, A. J. (2006) A newly designed microspectrofluorometer for kinetic studies on protein crystals in combination with X-ray diffraction. *Biophys. J.* Available electronically on May 12.
53. Gallivan, J. P., and Dougherty, D. A. (1999) Cation-π interactions in structural biology, *Proc. Natl. Acad. Sci. U.S.A. 96*, 9459−9464.
54. Wiegert, T., Sahm, H., and Sprenger, G. A. (1997) The substitution of a single amino acid residue (Ser-116 → Asp) alters NADP-containing glucose-fructose oxidoreductase of *Zymomonas mobilis* into a glucose dehydrogenase with dual coenzyme specificity, *J. Biol. Chem. 272*, 13126−13133.
55. Weiss, M. S., Brandl, M., Suhnel, J., Pal, D., and Hilgenfeld, R. (2001) More hydrogen bonds for the (structural) biologist, *Trends Biochem. Sci. 26*, 521−523.
56. Senes, A., Ubarretxena-Belandia, I., and Engelman, D. M. (2001) The Cα−H···O hydrogen bond: A determinant of stability and specificity in transmembrane helix interactions, *Proc. Natl. Acad. Sci. U.S.A. 98*, 9056−9061.
57. Duax, W. L., Pletnev, V., Addlagatta, A., Bruenn, J., and Weeks, C. M. (2003) Rational proteomics. I. Fingerprint identification and cofactor specificity in the short-chain oxidoreductase (SCOR) enzyme family, *Proteins 53*, 931−943.
58. Pierce, A. C., Sandretto, K. L., and Bemis, G. W. (2002) Kinase inhibitors and the case for CH···O hydrogen bonds in protein−ligand binding, *Proteins 49*, 567−576.
59. Vought, V., Ciccone, T., Davino, M. H., Fairbairn, L., Lin, Y., Cosgrove, M. S., Adams, M. J., and Levy, H. R. (2000) Delineation of the roles of amino acids involved in the catalytic functions of *Leuconostoc mesenteroides* glucose 6-phosphate dehydrogenase, *Biochemistry 39*, 15012−15021.
60. Arimitsu, E., Aoki, S., Ishikura, S., Nakanishi, K., Matsuura, K., and Hara, A. (1999) Cloning and sequencing of the cDNA species for mammalian dimeric dihydrodiol dehydrogenases, *Biochem. J. 342*, 721−728.

61. Asada, Y., Aoki, S., Ishikura, S., Usami, N., and Hara, A. (2000) Roles of His-79 and Tyr-180 of D-xylose/dihydrodiol dehydrogenase in catalytic function, *Biochem. Biophys. Res. Commun. 278*, 333−337.
62. Kühn, A. M. (2004) 1,5-Anhydro-D-fruktose-Reduktase aus Sinorhizobium morelense S-30.7.5: Isolierung, Charakterisierung, Überexpression in *E. coli* sowie Verwendung als neuer Biokatalysator, Ph.D. Thesis, Universität des Saarlandes, Saarbrücken, Germany.
63. Jez, J. M., Bennett, M. J., Schlegel, B. P., Lewis, M., and Penning, T. M. (1997) Comparative anatomy of the aldo-keto reductase superfamily, *Biochem. J. 326*, 625−636.
64. Karplus, P. A., and Schulz, G. E. (1989) Substrate binding and catalysis by glutathione reductase as derived from refined enzyme: Substrate crystal structures at 2 Å resolution, *J. Mol. Biol. 210*, 163−180.
65. Rao, S. T., and Rossmann, M. G. (1973) Comparison of supersecondary structures in proteins, *J. Mol. Biol. 76*, 241−256.
66. Fan, F., Lorenzen, J. A., and Plapp, B. V. (1991) An aspartate residue in yeast alcohol dehydrogenase I determines the specificity for coenzyme, *Biochemistry 30*, 6397−6401.
67. Hummel, W. (1997) New alcohol dehydrogenases for the synthesis of chiral compounds, *Adv. Biochem. Eng. Biotechnol. 58*, 145−184.
68. Radianingtyas, H., and Wright, P. C. (2003) Alcohol dehydrogenases from thermophilic and hyperthermophilic archaea and bacteria, *FEMS Microbiol. Rev. 27*, 593−616.
69. Filling, C., Berndt, K. D., Benach, J., Knapp, S., Prozorovski, T., Nordling, E., Ladenstein, R., Jornvall, H., and Oppermann, U. (2002) Critical residues for structure and catalysis in short-chain dehydrogenases/reductases, *J. Biol. Chem. 277*, 25677−25684.
70. Ghosh, D., Pletnev, V. Z., Zhu, D. W., Wawrzak, Z., Duax, W. L., Pangborn, W., Labrie, F., and Lin, S. X. (1995) Structure of human estrogenic 17β-hydroxysteroid dehydrogenase at 2.20 Å resolution, *Structure 3*, 503−513.
71. Birktoft, J. J., and Banaszak, L. J. (1983) The presence of a histidine-aspartic acid pair in the active site of 2-hydroxyacid dehydrogenases. X-ray refinement of cytoplasmic malate dehydrogenase, *J. Biol. Chem. 258*, 472−482.
72. Lodola, A., Shore, J. D., Parker, D. M., and Holbrook, J. (1978) Malate dehydrogenase of the cytosol. A kinetic investigation of the reaction mechanism and a comparison with lactate dehydrogenase, *Biochem. J. 175*, 987−998.
73. Cosgrove, M. S., Naylor, C., Paludan, S., Adams, M. J., and Levy, H. R. (1998) On the mechanism of the reaction catalyzed by glucose 6-phosphate dehydrogenase, *Biochemistry 37*, 2759−2767.
74. Cosgrove, M. S., Loh, S. N., Ha, J. H., and Levy, H. R. (2002) The catalytic mechanism of glucose 6-phosphate dehydrogenases: Assignment and ^{1}H NMR spectroscopy pH titration of the catalytic histidine residue in the 109 kDa *Leuconostoc mesenteroides* enzyme, *Biochemistry 41*, 6939−6945.
75. Chenault, H. K., and Whitesides, G. M. (1987) Regeneration of nicotinamide cofactors for use in organic synthesis, *Appl. Biochem. Biotechnol. 14*, 147−197.
76. Wong, C. H., and Whitesides, G. M. (1981) Enzyme-catalyzed organic synthesis: NAD(P)H cofactor regeneration by using glucose-6-phosphate and the glucose-5-phosphate dehydrogenase from *Leuconostoc mesenteroides*, *J. Am. Chem. Soc. 103*, 4890−4899.
77. Brunger, A. T. (1992) Free *R* value: A novel statistical quantity for assessing the accuracy of crystal structures, *Nature 355*, 472−475.
78. Rajashankar, K. R., Solorzano, V., Kniewel, R., and Lima, C. D. (2004) Crystal Structure of a Putative Oxidoreductase (Virulence Factor Mvim Homolog), (submitted for publication).
79. Sun, D., Sato, M., Yoshida, T., Shimizu, H., Miyatake, H., Adachi, S., Shiro, Y., and Kikuchi, A. (2000) Crystallization and preliminary X-ray diffraction analysis of a rat biliverdin reductase, *Acta Crystallogr. D56*, 1180−1182.
80. Gouet, P., Courcelle, E., Stuart, D. I., and Metoz, F. (1999) ESPript: Analysis of multiple sequence alignments in PostScript, *Bioinformatics 15*, 305−308.

BI052589Q